Transp Porous Med (2009) 76:449–469
DOI 10.1007/s11242-008-9257-1

A Model of Buoyancy-Driven Two-Phase Countercurrent Fluid Flow

Dmitriy Silin · Tad Patzek · Sally M. Benson

Received: 26 April 2007 / Accepted: 5 June 2008 / Published online: 25 July 2008

Abstract We seek simple analytical solutions in a model of gas flow driven by a combination of buoyancy, viscous, and capillary forces. Traveling-wave solutions describe propagation of the top and bottom of the gas plume. The top of the plume has low gas saturation, but propagates much faster than the bottom. The theoretical maximum of the velocity of propagation of the top of the plume provides a simple conservative estimate of the time until plume evolution will dramatically slow down. A sequence of rarefaction and traveling-wave solutions characterizes the transition zones between the top and bottom stable regions. The analytical results are applied to studying carbon dioxide flow caused by leaks from deep geological formations used for CO_2 storage. The results are also applicable for modeling flow of natural gas leaking from seasonal gas storage, or for modeling of secondary hydrocarbon migration.

Keywords Multiphase flow · Porous media · Gas migration · Darcy's law

1 Introduction

This work is motivated by the growing interest in injecting carbon dioxide into deep geological formations as a means of avoiding its atmospheric emissions and consequent global warming (IPPC 2005). While it is anticipated that CO_2 will remain trapped beneath the seal

D. Silin (✉)
Lawrence Berkeley National Laboratory, 1 Cyclotron Road, MS 90R1116, Berkeley, CA 94720, USA
e-mail: DSilin@lbl.gov

T. Patzek
University of California, Berkeley, 415 Davis Hall, Berkeley, CA 94720, USA
e-mail: patzek@patzek.berkeley.edu

S. M. Benson
Energy Resources Engineering Department, Stanford University, 074 Green Sciences Building, 367 Panama Street, Stanford, CA 94305-22020, USA
e-mail: SMBenson@stanford.edu

of the storage reservoir, it is important to have a good understanding of the rate that CO_2 would move upward under buoyancy forces should some of the CO_2 leak out of the storage reservoir. To date, studies of leakage have either focused on the role of leaking wells (Gasda et al. 2004; Nordbotten et al. 2005) or used numerical simulation to investigate leakage through poor-quality reservoir seals (Lindeberg 1997; Doughty and Myer 2008). Here, we are interested in the fate of CO_2 driven upward by buoyancy, using analytical methods to help provide insights into the physics of countercurrent flow of CO_2 and water and to bound potential migration rates.

In a steady-state flow, two immiscible fluids saturating a porous medium approach an equilibrium distribution characterized by a local minimum of the surface tension energy. Although the capillary forces act locally at a microscopic scale, they constrain the macroscopic flow by arranging the distribution of the fluids. Examples of such flows are oil and gas migration (Hubbert 1953; Muskat 1949), or the flow of gas leaking from an underground storage into an overlying aquifer. Early works (Rapoport 1955; Mattax and Kyte 1962) report experimental and theoretical studies of countercurrent two-phase flow in porous media in the context of enhanced oil recovery.

A number of researchers have studied models of buoyancy-driven vertical migration of fluids in the past using both analytical and numerical approaches. Shvidler and Levi (1970) have obtained an analytical solution to a static gravity segregation problem and numerically investigated dynamic gravity-driven vertical two-phase fluid flow. More recently, similar problems have been studied in the contexts of formation of oil and gas reservoirs by secondary hydrocarbon migration (Siddique and Lake 1997; Bedrikovetsky et al. 2001) and gravity-drainage in fractured reservoirs (Luan 1994). An analytical solution for a model of gas plume propagation in a saline aquifer caused by gas injection has been obtained by Nordbotten et al. (2005). Their solution is based on the Buckley–Leverett approximation (Buckley and Leverett 1942), where capillarity is neglected. Doughty has investigated numerically the impact of capillary hysteresis effects on CO_2 migration (Doughty 2007). Riaz and Tchelepi (2006) have numerically investigated a problem very similar to the one considered in this work with analytical tools.

In this study, we focus on a case where a less dense nonwetting fluid, e.g., gas, migrates vertically upward in an initially dense-liquid-saturated reservoir. We focus on the relative impact of gravity, capillarity, and viscosity on the plume dynamics, and assume that the formation is homogeneous. In general, vertical fluid migration is significantly affected by the rock heterogeneity. For instance, if the formation has a system of vertical or inclined conductive fractures or faults, the leaking gas, most likely, will flow through this system. We also assume that the domain under consideration is deep enough so that the gas is supercritical and variations of the density of gas and the viscosities of both fluids can be neglected. In this study, we neglect processes like fluid exchange by evaporation and condensation, as well as precipitation and dissolution.

We employ analytical tools, for which we assume an idealized homogeneous formation. We simplify the model so that the interactions between the driving forces do not interfere with other phenomena. Our principal finding is that the evolution of the saturation profile of a moving plume can be described as a sequence of traveling and rarefaction waves, as presented in Fig. 1. The model predicts that two traveling waves characterize the evolution of the top and bottom boundaries of the saturation profile. The top of the plume has low gas saturation, but propagates much faster than the bottom. Thus, the plume stretches until it either reaches a uniform residual gas saturation or reaches a seal. The model also suggests that there is a fixed depth at which the fluid saturation remains constant most of the time. Above this point, the migrating gas displaces water by drainage. Below this point, where most gas is at the

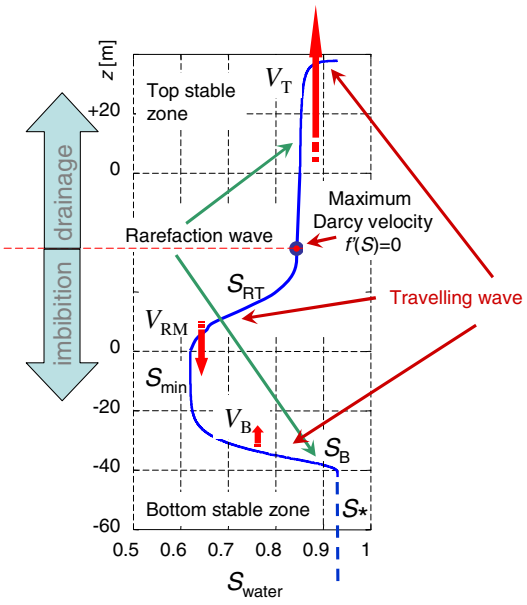

Fig. 1 The top part of the plume is relatively "lean" with respect to the gas saturation, but propagates much faster than the bottom part saturated with gas

beginning, the fluid displacement mechanism is imbibition. In addition, this stable point is characterized by the most intense countercurrent fluid flow. From the relative permeability curves, we estimate the theoretical maximum of the plume propagation velocity. This simple estimate can be used for prediction of the time of plume evolution.

Accurate prediction of plume evolution requires knowledge of the fluid and formation properties. We have found that the usually used capillary pressure parametrization proposed in Van Genuchten (1980) is insufficient for an adequate fitting of the laboratory-measured capillary pressure for the Frio formation sandstone. In this study, we have developed a different parametrization, which is described in Appendix A. The selection of the Frio formation properties has been motivated by the fact that it was the site of a pilot CO_2 injection test. Papers Daley et al. (2007) and Doughty et al. (2008) provide a comprehensive overview of that project.

The paper is organized as follows. First, we briefly review the gravity-segregation model and formulate the main equations of countercurrent flow of gas and brine. Applying this model to describe vertical gas plume migration, we characterize different zones of the plume by traveling-wave and rarefaction-wave solutions. Conclusions are given at the end. Physical parameters used in the case studies presented in this paper are gathered in Appendix A. Appendix B describes the traveling-wave and rarefaction-wave solutions.

2 The Model

In this section, we review the principal equations of the mathematical model of buoyancy-driven countercurrent flow. We neglect the lateral flow components, and so the flow is essentially vertical. This assumption is valid if the gas flow is horizontally confined by fracture walls or if we consider fluid flow far away from the lateral boundaries of the plume. Under these assumptions, the two-phase fluid flow is countercurrent: in a representative elementary

volume, the gas flowing upward is replaced by an equal volume of the brine flowing downward. These assumptions make our model similar to the one developed by Luan (1994). We apply this model to study the evolution of the vertical saturation profile in a gas plume.

p_g and p_w denote the gas and brine pressures, respectively. The capillary pressure, $p_c = p_g - p_w$, is related to the local-equilibrium fluid distribution in the pore space. It is usually expressed as a function of saturation S, i.e., the fractional volume of the pore space filled with the water (Leverett 1941):

$$p_g - p_w = p_c(S) \tag{1}$$

This dependence on S is not a one-to-one correspondence (Muskat 1949), but is strongly affected by the history of fluid migration. Numerous studies emphasize differences between the drainage and imbibition capillary pressure curves (see Doughty 2007; Al-Futaisi and Patzek 2003; Al-Futaisi and Patzek 2004, and the references therein).

The permeability to each fluid is determined by the geometry of the part of the pore space occupied by this fluid. Hence, the remarks regarding history-dependence of the capillary pressure curve equally apply to the relative permeability curves: the permeability to each fluid is a function of both the liquid saturation and the history of the fluid migration. The velocity of propagation of the plume is determined by the velocity of propagation of its leading tip, where the fluid displacement mechanism is drainage. In order to simplify the calculations, we will use the drainage capillary pressure and relative permeability coefficients, $k_{rg} = k_{rg}(S)$ and $k_{rw} = k_{rw}(S)$, for the entire plume.

For each fluid phase, Darcy's law with an account for gravity yields (Hubbert 1956):

$$\mathbf{u}_g = \frac{k_{rg}(S)k}{\mu_g}\left(-\nabla p_g + \varrho_g \mathbf{g}\right) \tag{2}$$

$$\mathbf{u}_w = \frac{k_{rw}(S)k}{\mu_w}\left(-\nabla p_w + \varrho_w \mathbf{g}\right) \tag{3}$$

Here, $\mathbf{u}_g$ and $\mathbf{u}_w$ are, respectively, Darcy velocities or volumetric fluxes of the gas and liquid, μ_g and μ_w are the dynamic viscosities of the fluids, and ϱ_g and ϱ_w are their densities. The gravity acceleration is denoted by $\mathbf{g}$. Using Eq. 1, the liquid pressure p_w can be eliminated from the system of Eqs. 2 and 3:

$$\mathbf{u}_w = \frac{k_{rw}(S)k}{\mu_w}\left(-\nabla p_g + \nabla p_c(S) + \varrho_w \mathbf{g}\right) \tag{4}$$

The mass balance of gas and liquid can be expressed as

$$\frac{\partial\left(\varrho_g(1-S)\phi\right)}{\partial t} + \nabla \cdot (\varrho_g \mathbf{u}_g) = 0 \tag{5}$$

$$\frac{\partial(\varrho_w \phi S)}{\partial t} + \nabla \cdot (\varrho_w \mathbf{u}_w) = 0 \tag{6}$$

The porosity ϕ accounts only for the void space available for fluid flow. The total number of unknown functions is equal to 11: $\mathbf{u}_i$, p_i, ϱ_i $(i = g, w)$, and S. In order to determine a unique solution, Eqs. 1–6 must be complemented with two equations of state, one for each fluid, and with a consistent set of boundary and initial conditions.

We consider a spontaneous buoyancy-driven flow at a depth where carbon dioxide is in a supercritical state. The total interval where the solution is defined is not large relative to the absolute depth, and so the variation of the hydrostatic pressure is not large. With this

assumption, we neglect the compressibility of the fluids and rock and summation of Eqs. 5 and 6 yields

$$\nabla \cdot \left(\mathbf{u}_{\mathrm{g}} + \mathbf{u}_{\mathrm{w}}\right) = 0 \tag{7}$$

The flow is vertical, and there is no flow outside the plume. Hence, Eq. 7 implies that the magnitudes of fluid velocities satisfy

$$u_{\mathrm{g}} + u_{\mathrm{w}} = 0 \tag{8}$$

In other words, the flow is countercurrent (Barenblatt and Gilman 1987; Ryzhik 1960; Silin and Patzek 2004). Equations 1, 2, and 4 imply

$$\frac{\partial}{\partial z} p_{\mathrm{g}} = \frac{\dfrac{k_{\mathrm{rw}}(S)}{\mu_{\mathrm{w}}}}{\dfrac{k_{\mathrm{rw}}(S)}{\mu_{\mathrm{w}}} + \dfrac{k_{\mathrm{rg}}(S)}{\mu_{\mathrm{g}}}} \left[\frac{\partial}{\partial z} p_{\mathrm{c}}(S) - (\varrho_{\mathrm{w}} - \varrho_{\mathrm{g}})g\right] - \varrho_{\mathrm{g}} g \tag{9}$$

and

$$\frac{\partial}{\partial z} p_{\mathrm{w}} = -\frac{\dfrac{k_{\mathrm{rg}}(S)}{\mu_{\mathrm{g}}}}{\dfrac{k_{\mathrm{rw}}(S)}{\mu_{\mathrm{w}}} + \dfrac{k_{\mathrm{rg}}(S)}{\mu_{\mathrm{g}}}} \left[\frac{\partial}{\partial z} p_{\mathrm{c}}(S) - (\varrho_{\mathrm{w}} - \varrho_{\mathrm{g}})g\right] - \varrho_{\mathrm{w}} g \tag{10}$$

Here, g is the scalar magnitude of the gravity acceleration and z is the vertical coordinate directed upward. By virtue of Eq. 10, the Darcy velocity of water, Eq. 3, becomes

$$u_{\mathrm{w}} = \frac{k}{\mu_{\mathrm{w}}} f(S) \left[\frac{\partial}{\partial z} p_{\mathrm{c}}(S) - (\varrho_{\mathrm{w}} - \varrho_{\mathrm{g}})g\right] \tag{11}$$

where

$$f(S) = \frac{k_{\mathrm{rw}}(S)\dfrac{k_{\mathrm{rg}}(S)}{\mu_{\mathrm{g}}}}{\dfrac{k_{\mathrm{rw}}(S)}{\mu_{\mathrm{w}}} + \dfrac{k_{\mathrm{rg}}(S)}{\mu_{\mathrm{g}}}} = \frac{k_{\mathrm{rw}}(S)}{\dfrac{k_{\mathrm{rw}}(S)}{k_{\mathrm{rg}}(S)}\dfrac{\mu_{\mathrm{g}}}{\mu_{\mathrm{w}}} + 1} \tag{12}$$

In Eq. 11, we have left mobility factor k/μ_{w} outside the function $f(S)$ to make the latter dimensionless.

Substitution of Eq. 11 into Eq. 6 yields

$$\frac{\partial(\phi S)}{\partial t} = -\frac{\partial}{\partial z}\left(\frac{k}{\mu_{\mathrm{w}}} f(S)\left(\frac{\partial}{\partial z} p_{\mathrm{c}}(S) - (\varrho_{\mathrm{w}} - \varrho_{\mathrm{g}})g\right)\right) \tag{13}$$

2.1 Flow Equations in a Dimensionless Form

Let H denote the thickness of the aquifer. Then, dimensionless vertical coordinate and time, ζ and τ, can be introduced in the following way:

$$\zeta = \frac{z}{H} \quad \text{and} \quad \tau = \frac{k\left(\varrho_{\mathrm{w}} - \varrho_{\mathrm{g}}\right) g}{\mu_{\mathrm{w}} H}\, t \tag{14}$$

In these variables, the dimensionless Darcy velocity of water W_w has the following form:

$$W_w = \frac{\mu_w}{k(\varrho_w - \varrho_g)g} u_w = f(S)\left[\frac{1}{(\varrho_w - \varrho_g^*)g}\frac{\partial}{\partial z} p_c(S) - 1\right] \tag{15}$$

The capillary pressure function can be expressed through dimensionless Leverett's $\mathcal{J}$-function (Leverett et al. 1942):

$$p_c(S) = \sigma\sqrt{\frac{\phi}{k}}\mathcal{J}(S) \tag{16}$$

where σ is the surface tension coefficient at the water–gas interface. Thus, Eqs. 13 and 15 take the form

$$\phi\frac{\partial S}{\partial \tau} = -\frac{\partial}{\partial \zeta} W_w \tag{17}$$

and

$$W_w = f(S)\left(\gamma\mathcal{J}'(S)\frac{\partial S}{\partial \zeta} - 1\right) \tag{18}$$

where

$$\gamma = \frac{\sigma}{(\varrho_w - \varrho_g)gH}\sqrt{\frac{\phi}{k}} \tag{19}$$

The dimensionless factor γ is analogous to the reciprocal Bond number and evaluates the ratio between the capillary and buoyancy forces. Its value is of the order of 1 for carbon dioxide flowing in a 20-m-thick aquifer layer of permeability of the order of 100 millidarcy and porosity about 20% at a depth of several kilometers. However, the magnitude of γ is much larger in a thin low-permeability seal. For instance, if the permeability is of the order of 0.01 millidarcy, the porosity is around 1%, and the thickness is of the order of 1 m; then, $\gamma = 10^3$, which is three orders of magnitude larger than in an aquifer. With the same values of the fluid and porous medium parameters, the characteristic plume propagation time in the above-mentioned permeable aquifer is measured in weeks, whereas for a tight seal, this time scale is of the order of hundreds or thousands of years.

Equations 17 and 18 can be summarized in the form of a nonlinear diffusion–advection equation

$$\phi\frac{\partial S}{\partial \tau} = \frac{\partial}{\partial \zeta}\left[f(S)\left(-\gamma\mathcal{J}'(S)\frac{\partial S}{\partial \zeta} + 1\right)\right] \tag{20}$$

2.2 Three Asymptotic Forms of Eq. 20

Equation 20 resembles Rappoport–Leas water–oil displacement equation (Barenblatt et al. 1990). This analogy suggests three asymptotic approximations, depending on the relative values of the two terms in the parentheses on the right-hand side. If

$$\left|\gamma\mathcal{J}'(S)\frac{\partial S}{\partial \zeta}\right| \gg 1 \tag{21}$$

then the flow can be characterized by Ryzhik's self-similar solution (Ryzhik 1960; Barenblatt et al. 1990). A condition like 21 holds where the saturation changes abruptly, for example, at the gas–water interface near the leading front of a plume entering a low-permeability seal.

In the second case, the flow is considered in a permeable thick aquifer, so that

$$\left|\gamma \mathcal{J}'(S)\frac{\partial S}{\partial \zeta}\right| \sim 1 \tag{22}$$

In this case, neither gravity forces nor capillarity can be neglected and two stable zones at the top and at the bottom of the plume can be described by traveling-wave solutions.

Small saturation gradient, so that

$$\left|\gamma \mathcal{J}'(S)\frac{\partial S}{\partial \zeta}\right| \ll 1 \tag{23}$$

leads to the Buckley–Leverett approximation. In this case, the Darcy velocities of the fluids do not depend on capillary pressure,

$$W_{\mathrm{w}} = -f(S) \tag{24}$$

and Eq. 20 reduces to a hyperbolic equation

$$\phi\frac{\partial S}{\partial \tau} = \frac{\partial}{\partial \zeta} f(S) \tag{25}$$

Known solutions to hyperbolic equations include shock or rarefaction waves (Buckley and Leverett 1942; Barenblatt et al. 1990). By introducing a new variable,

$$U(\zeta,\tau) = \phi\int_0^{\zeta} S(\eta,\tau)\,\mathrm{d}\eta \tag{26}$$

which evaluates the mean volume of water relative to the bulk volume of the porous medium, one obtains a Hamilton–Jacobi equation

$$\frac{\partial U}{\partial \tau} = f\left(\frac{\partial U}{\partial \zeta}\right) \tag{27}$$

Development of shock waves in Buckley–Leverett theory is equivalent to the loss of smoothness of the solution to a Hamilton–Jacobi equation. The latter leads to the concept of viscosity solution (Crandall et al. 1984).

One can demonstrate that the convexity or concavity of the function f and the initial condition for U determine whether the solution remains smooth or the evolution of the saturation profile may lead to development of shock waves (Silin 1997, 1998). A rarefaction-wave solution is smooth in ζ for all τ. It is feasible only on a saturation interval, where the monotonicity of the initial saturation profile and the convexity of function f are the right combination. For example, if U at $\tau = 0$ is a concave function of ζ, which is the case if water saturation increases with depth, then concavity of $f(S)$ guarantees that the respective solution is smooth at all times.

A shock wave is an asymptotic solution implied by neglecting the transition zone at the gas–water displacement front. Such a solution is justified in water–oil displacement models with a high flow rate, which must be forced by injection (Barenblatt et al. 1990). In our model, the flow rate cannot be forced, and depending on the magnitude of dimensionless factor γ, such an approximation may lead to inadequate conclusions. Therefore, we simulate the evolution of gas–water transition zones using the full traveling-wave solutions to Eq. 20. Such an approach excludes shocks and makes possible estimation of the thicknesses of transition zones (see Appendix B).

2.3 The Structure of the Plume

We model the evolution of a vertically migrating plume of gas by splitting it into several zones. In each zone, the saturation profile is described by a simple analytical solution, which is either a traveling-wave or a rarefaction wave. Both types of solutions are described in Appendix B. These solutions are asymptotic, and therefore, are meaningful only within certain length and time scales. Since these scales are not identical for both types of solutions, conditions must be established guaranteeing continuity of the plume. Each solution automatically satisfies mass conservation. Hence, compatibility conditions are derived from the requirement of equal propagation: the speed of propagation of the top or bottom tip of a rarefaction wave must match the speed of propagation of the adjacent traveling-wave. This requirement provides a set of conditions linking different parts of the plume. Satisfying these conditions leads to building of the whole plume as a sequence of blocks (see Fig. 1). Some of these blocks may shrink to zero as the plume evolves. Depending on the initial saturation distribution in the plume, not all of these blocks are necessarily present from the very beginning. Figure 2 shows an example of calculation of the plume evolution in four-month time increments for the parameters given in Table 1. At the beginning, the rarefaction wave at the tale of the plume, symbolically shown as a broken line, is a negligibly small part of the entire profile. With time, the low-water (i.e., high-gas) saturation zone of the plume will disperse and this tail rarefaction wave will stretch over the whole low-gas saturation plume.

Water saturation profile, $S(\xi, \tau)$, is the key unknown function. All other parameters can be found from $S(\xi, \tau)$. Indeed, the gradient of water saturation can be evaluated without differentiation using Eq. B.12. The Darcy velocity is readily obtained by substitution of this gradient into Eq. 18. Water pressure can be obtained by converting the dimensionless Darcy

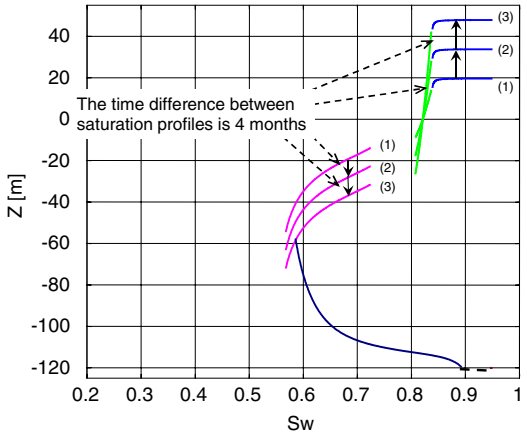

Fig. 2 Evolution of water saturation profile in the plume. The origin, $z = 0$, is associated with the center of the rarefaction wave at the top of the plume

Table 1 Formation and fluid parameters used in the calculations

Absolute permeability in aquifer, k	100 millidarcy
Porosity in aquifer, ϕ	20%
Water viscosity, μ_w	$5.0 \cdot 10^{-4}$ Pa-s
Gas viscosity, μ_g	$4.38 \cdot 10^{-5}$ Pa-s
Water density, ϱ_w	$1.0 \cdot 10^{3}$ kg/m^3
Gas density, ϱ_g	$0.561 \cdot 10^{3}$ kg/m^3
Surface tension coefficient, σ	$3 \cdot 10^{-2}$ N/m

velocity back into physical units and integrating Eq. 10. Gas pressure is evaluated using the capillary pressure curve, Eq. 1.

The following subsections describe individual blocks of the plume. The values of physical parameters used in the calculations are discussed in Appendix A.

2.4 Traveling-Wave at the Top of the Plume

The top of the plume can be characterized by a traveling-wave solution. Above the plume, the formation is saturated with brine. Thus, $S_2 = 1$ in Eq. B.6. Since $f(1) = 0$, Eq. B.8 reduces to

$$V(S) = \frac{f(S)}{\phi(1-S)} \tag{28}$$

where S is the saturation near the top of the plume. Function $V(S)$ attains a maximum, which defines the theoretical upper limit for the velocity of plume migration (see Fig. 3). Let us denote the respective saturation by S_T. The sharp shape of the $V(S)$ curve is a consequence of the significant viscosity contrast between water and gas. In case of hydrocarbon migration, this contrast may be significantly lower. Therefore, the respective curve will be smoother and the maximum will shift toward a lower water saturation (see Fig. 4).

At the leading tip of the plume, the saturation behind the front must correspond to the maximum of velocity (28), S_T. If it were less than S_T, the very top of the plume would run away and disperse, and a new front would develop. If the saturation behind the front exceeded S_T, then small heterogeneities and consequent saturation fluctuations would create a faster-propagating front that would coalesce with the top of the plume.

By selecting some $S_0 > S_T$, and respective dimensionless depth ξ_0, Eq. B.15 reduces to

$$\xi(S) = \xi_0 + \int_{S_0}^{S} \frac{\gamma f(\eta)\mathcal{J}'(\eta)}{f(\eta) - \dfrac{f(S_T)}{1-S_T}(1-\eta)}\,\mathrm{d}\eta \tag{29}$$

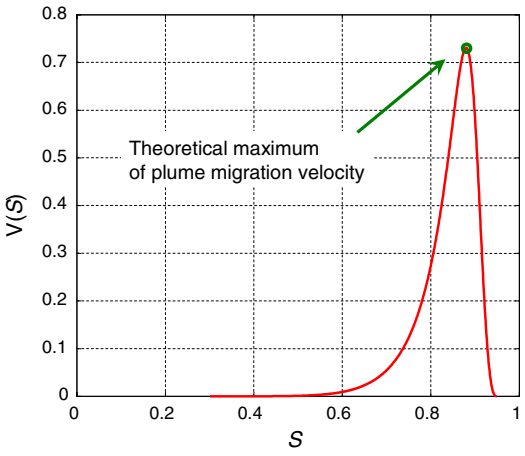

Fig. 3 The maximum of the $V(S)$ curve defines the theoretical maximum of the plume propagation velocity

By virtue of Eq. 28, the latter equation is equivalent to

$$\xi(S) = \xi_0 + \int_{S_0}^{S} \frac{\gamma \mathcal{J}'(\eta)}{1 - \dfrac{V(S_T)}{V(\eta)}} \, \mathrm{d}\eta \tag{30}$$

By the definition of saturation S_T, the denominator of the integrand is negative, and so is the numerator. Thus, the whole expression is positive and water saturation increases with ξ. The interval of saturations, where Eq. 30 is valid, does not include singularity points of the Leverett's function. In particular, such an interval must be strictly between the end-point saturations.

The asymptotic character of this solution is revealed by the fact that the integrand has a singularity as the dummy variable η approaches S_T. Consequently, the transition part of the profile is followed by a theoretically infinite interval of almost constant saturation. However, such constant-saturation parts of the plume are not sustainable: local heterogeneities inevitably result in the development of new fronts with transition zones. A stable solution is obtained by linking the top traveling-wave transition part of the plume to a rarefaction wave that follows behind.

2.5 The Rarefaction Wave behind the Leading Part of the Plume

The velocity of propagation of the top of the plume is characterized by the maximum of the function $V(S)$ (Eq. 28). At the maximum, $V'(S) = 0$ and $V''(S) \leq 0$. Hence,

$$f'(S)\big|_{S=S_T} = -\frac{f(S)}{1-S}\bigg|_{S=S_T} \quad \text{and} \quad f''(S)\big|_{S=S_T} < 0 \tag{31}$$

The left-hand equality in Eq. 31 means that the velocity of propagation of the top of the plume automatically matches the velocity of propagation of the rarefaction wave with saturation S_T at the top (see Eq. B.19). The right-hand inequality implies that $f(S)$ is a concave function of S near $S = S_T$ (Rockafellar 1970). Hence, this rarefaction wave corresponds to the interval of concavity of the function $f(S)$ (see Fig. 5).

Let S_{RT} be the brine saturation at the lower end of the rarefaction wave and S_M be the saturation at which the function $f(S)$ attains its maximum. We assume that $S_{RT} < S_M$. By

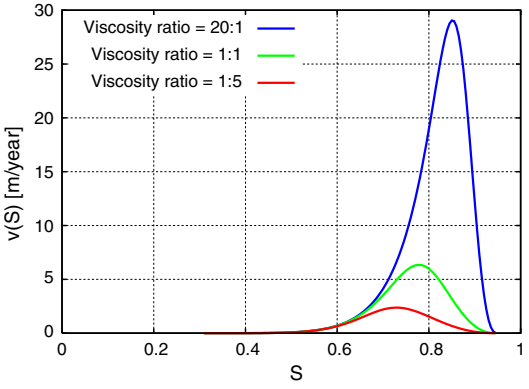

Fig. 4 Plume migration velocity in m/year for three different viscosity ratios μ_w:μ_g

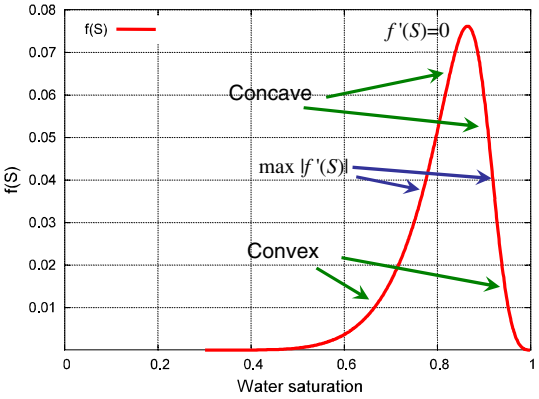

Fig. 5 Plot of $f(S)$: normally the plot includes an interval of concavity between two intervals where the function is convex

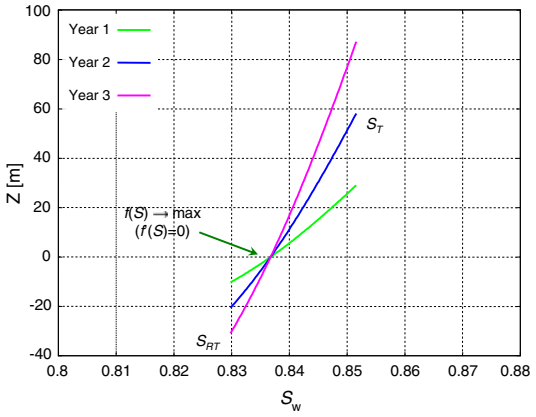

Fig. 6 Evolution of a rarefaction wave

virtue of Eq. B.18, the top and bottom bounds of the rarefaction zone, $\zeta_{\mathrm{T}}(\tau)$ and $\zeta_{\mathrm{RT}}(\tau)$, are characterized by

$$\zeta_{\mathrm{T}}(\tau) = \zeta_0 - \tau \frac{f'(S_{\mathrm{T}})}{\phi} = \zeta_0 + \tau V(S_{\mathrm{T}}) \quad \text{and} \quad \zeta_{\mathrm{RT}}(\tau) = \zeta_0 - \tau \frac{f'(S_{\mathrm{RT}})}{\phi} \tag{32}$$

Note the opposite directions of propagation: the top end moves upward, along with the leading part of the plume, and the bottom one moves downward (see Fig. 6). The Darcy velocity of the fluids inside the rarefaction wave is defined by Eq. 24. Therefore, the magnitude of Darcy velocity attains its greatest value at the saturation $S = S_{\mathrm{M}}$. At this saturation, the derivative $f'(S)$ vanishes, which corresponds to the vertical coordinate ζ_0, where the saturation is constant. Thus, the most intense fluid flow happens in the immobile part of the saturation profile! Above this point, the brine saturation decreases, and so the fluid displacement mechanism is drainage. Below ζ_0, the brine saturation increases, and so the fluid displacement is imbibition.

The assumption $S_{\mathrm{RT}} < S_{\mathrm{M}}$, in particular, imply that $f'(S_{\mathrm{RT}}) > 0$. At the same time, for the rarefaction-wave solution to exist, S_{RT} must be inside or at the end of an interval of concavity of function $f(S)$. If the minimum of water saturation in the plume, $S_{\min}$, is outside this interval, then the rarefaction wave is followed by a traveling-wave front moving downward and S_{RT} must be determined from matching the velocities of propagation (see next subsection).

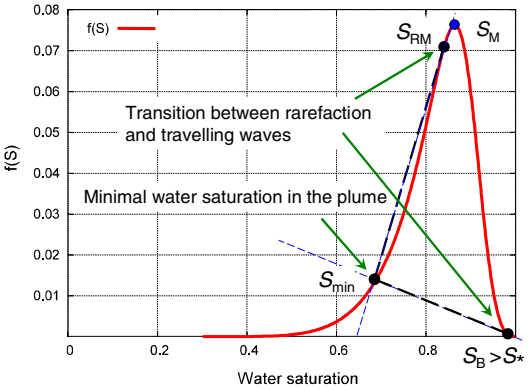

Fig. 7 Saturations at the tail of rarefaction wave and the main part of the plume: the saturation at the transition point, S_{RM}, is the tangential point between the plot of $f(S)$ and a straight line passing through S_{min}. The transition saturation, S_{B}, between the traveling and rarefaction waves at the bottom can be determined in a similar way

2.6 The Main Part of the Plume

The main part of the plume is characterized by the maximum gas saturation and minimum water saturation: $S = S_{\mathrm{min}}$. The dynamics of saturation profile evolution behind the rarefaction wave zone can be characterized by a traveling-wave solution. By virtue of Eq. B.8, with $S_1 = S_{\mathrm{min}}$ and $S_2 = S_{\mathrm{RT}}$, the dimensionless velocity

$$V_{\mathrm{min}} = -\frac{1}{\phi}\frac{f\left(S_{\mathrm{RT}}\right) - f\left(S_{\mathrm{min}}\right)}{S_{\mathrm{RT}} - S_{\mathrm{min}}} \tag{33}$$

is negative and the traveling-wave propagates *downward*. In particular, the fluid displacement mechanism is imbibition. Matching the derivative of ξ_{RT} from the rarefaction wave above with velocity (33) leads to

$$f'(S_{\mathrm{RT}}) = \frac{f\left(S_{\mathrm{RT}}\right) - f\left(S_{\mathrm{min}}\right)}{S_{\mathrm{RT}} - S_{\mathrm{min}}} \tag{34}$$

The latter equation determines S_{RT}. In Fig. 7, the straight line with the slope $f'(S_{\mathrm{RT}})$ is tangential to the plot $f(S)$ at $S = S_{\mathrm{RT}}$ and it must cross the plot at $S = S_{\mathrm{min}}$. Clearly, as S_{min} approaches the dividing point between the intervals of convexity and concavity of function $f(S)$, the solution to Eq. 34, S_{RT}, converges to the same dividing point as well. At the exact limit, when $S_{\mathrm{min}} = S_{\mathrm{RT}}$, the downward traveling-wave disappears. Therefore, this downward traveling-wave can be present only if the function $f(S)$ is convex near $S = S_{\mathrm{min}}$.

2.7 Saturation Distribution in the Tail of the Plume

Gas saturation behind the plume is not zero, but the fluids do not flow because the gas phase becomes disconnected. Let us denote by S_{rg} the residual gas saturation behind the plume and put

$$S_* = 1 - S_{\mathrm{rg}} \tag{35}$$

Similar to the upper part of the plume, the evolution of the saturation profile at the bottom can be characterized by a traveling-wave followed by a rarefaction wave. Let S_{B} be water

saturation at the transition point. Then, by virtue of Eq. B.8, the velocity of propagation of the bottom traveling-wave, V_B, is

$$V_B = -\frac{1}{\phi}\frac{f(S_B) - f(S_{min})}{S_B - S_{min}} \tag{36}$$

V_B is positive, and therefore the propagation of the wave is upward and the fluid displacement mechanism is imbibition. Matching the velocity V_B with the velocity of the top end of the following rarefaction wave yields the equation

$$f'(S_B) = \frac{f(S_B) - f(S_{min})}{S_B - S_{min}} \tag{37}$$

(see Eq. B.19). Thus, the saturation S_B characterizes the tangential point between the straight line, which intersects the plot of $f(S)$ at $S = S_{min}$, and the plot of $f(S)$ (Fig. 7). Although $S_B > S_*$, the difference between the two saturations is tiny. Therefore, the role of the rarefaction wave in the entire saturation profile is small as long as the maximal gas saturation in the main plume is relatively high. The bottom end of this rarefaction wave is where water saturation is equal to S_*. In particular, $f'(S_*) = 0$, and only the upper boundary of the bottom rarefaction wave moves.

2.8 Further Remarks

The calculations presented above suggest the gas plume in a brine-saturated aquifer can be modeled as a sequence of traveling and rarefaction waves. Driven by buoyancy, the plume propagates by stretching vertically upward, unlike a gas bubble in bulk water. The velocities of propagation of the fronts described by traveling-wave solutions are determined from the conservation of mass and are functions of the saturations ahead of and behind the front. As the saturation profile evolves, these saturations may change. For example, the saturations above and below the intersection of the bottom profile with profiles (1)–(3) in Fig. 2 are not equal. We have neglected these end saturation variations. Such a simplification may be unacceptable when the variations of end saturations are significant. However, it affects only the internal structure of the plume, not the profile at the leading front. The velocity of propagation of the latter eventually determines the time of plume stretching.

If the initial gas saturation in the plume is low, the flow pattern is different. Although such a case is of lesser practical interest, we briefly discuss it here. The case where $S_{RT} < S_{min} < S_M$ is similar to the case $S_{min} = S_{RT}$ considered above: the downward traveling-wave is not present and the bottom end of the rarefaction wave propagates downward until it meets the bottom traveling-wave and the plume collapses.

An interesting case is $S_{min} = S_M$. By Eq. 32, the bottom boundary of the rarefaction wave does not move and the plume collapses when the bottom traveling-wave passes the location where $f'(S) = 0$.

If $S_M < S_{min} < S_T$, then both ends of the rarefaction wave behind the leading part of the plume propagate upward. The saturation S_B can be significantly different from S_*. The magnitude of the velocity of the bottom of the plume is characterized by the slope of the line between points with coordinates $(S_{min}, f(S_{min}))$ and $(S_B, f(S_B))$ (Fig. 7). Thus, unlike the practically zero propagation velocity at the bottom of the plume at high gas saturations, in this case, this velocity is relatively high. If

$$-f'(S_B) > \frac{f(S_T)}{1 - S_T} \tag{38}$$

the bottom velocity exceeds $V(S_T)$. The inequality (38) can be satisfied only when gas saturations are low. For example, at later times, when the gas saturation becomes small in the whole plume, the bottom traveling-wave will accelerate and will eventually stretch the plume to uniform residual saturation.

The above calculations above assumed that the formation is initially fully water-saturated. However, if the plume follows behind other plumes, the water saturation at the front of the plume is not one but corresponds to the residual gas saturation behind the other plumes. If the upper plume has already stretched to uniform residual gas saturation, then, by Eq. B.8, the dimensionless velocity of propagation of the top of the following plume is given by equation

$$V_F(S) = \frac{f(S)}{1 - S_* - S} \tag{39}$$

Clearly, $V_F(S) > V(S)$. Thus, the "follow-up" plumes propagate faster than the first one. In particular, subsequent plumes following one another will likely coalesce after some time.

The fluid displacement mechanism in the part of the plume at initially high gas saturation is imbibition. That is, water displaces supercritical gas. At the top, a low-saturation gas flow displaces the reservoir water. The theory of front stability in two-phase fluid displacement is based on pressure perturbations (Saffman and Taylor 1958; Homsy 1987). Thus, it is not applicable to buoyancy-driven countercurrent flow. Pressure perturbations in each fluid are possible only if the saturation changes. Water saturation behind the front determines the velocity of propagation (Eq. 28). Since the derivative of $V(S)$ vanishes at $S = S_T$, a small perturbation of the saturation behind the front, $\widetilde{S} = S_T + \delta S$, results in a variation of the front propagation velocity of the order $O(\delta S^2)$. Thus, perturbations of the saturation may generate some dispersion of the front. However, development of instabilities like macroscopic viscous fingers is unlikely. This observation becomes less counterintuitive once one notices that the mobility contrast at the front is close to one due to the low gas saturation. Based on the results of 2D numerical simulations of buoyancy-driven countercurrent flow, similar to the one considered in this study, Bryant et al. (2006) conclude that plume dispersion can develop due to formation heterogeneity. However, no viscous fingers have been produced by the simulations.

At the pore scale, countercurrent flow consists of numerous flow channels and pathes, where the fluids flow in the opposite directions. If the permeability of the formation is high enough, the buoyancy drive can become sufficient to support a nonzero macroscopic *curl* flow. Such a flow is not countercurrent and the argument above is not applicable. An extreme case of high permeability is bulk fluid flow, where the front is unstable.

2.9 A Simple Estimate of Plume Migration Time

A rough estimate of the time needed to trap all the gas initially contained in the plume can be obtained as follows. Due to the high viscosity contrast, the difference between S_T and S_* is not very large. Viscosity contrast also implies that the function $V(S)$ decreases sharply as S deviates from S_T. Once water saturation at the top of the plume becomes larger than S_T, its propagation slows down dramatically. Further plume stretching happens at low gas saturation and decelerates continuously. The active plume stretching continues until water saturation in the plume becomes close to S_T. If the initial thickness of the plume is L, then mass balance yields an expression for the stretched plume thickness in the form: $L_T = \frac{1 - S_{\min}}{1 - S_T} L$. Since

the velocity of plume stretching is approximately equal to the velocity of propagation of the top, $V(S_T)$, the time to attain this thickness is approximately

$$t \approx \frac{\phi \mu_w L}{k(\varrho_w - \varrho_g)g} \frac{S_T - S_{min}}{f(S_T)} \tag{40}$$

Here, we have used the scaling of the velocity into physical units provided by Eq. B.2.

3 Conclusions

Interactions of buoyant, capillary, and viscous forces determine the spontaneous flow of a gas plume in an aquifer. We focus on vertical flow, assuming either flow in a vertical fracture or flow in the central part of a large plume away from the lateral boundaries. The two-phase flow is countercurrent, where a volume of one fluid replaces an equal volume of the other one.

The evolution of a gas plume can be modeled as a sequence of traveling and rarefaction waves. In a traveling-wave, the capillary pressure function defines the thickness of a stable transition zone in the vertical saturation profile. In a rarefaction wave zone, the saturation variation can only decrease, and therefore the impact of capillarity is neglected.

The top and the bottom of the plume are modeled as traveling-waves. At high viscosity contrast between gas and water, the wave velocity at the bottom part is negligibly small relative to the speed of propagation at the top. Therefore, the plume does not rise like a bubble in bulk water, but stretches until it reaches a uniform residual gas saturation or hits a horizontal seal. The theoretical maximum of velocity of the top of the plume propagation determines how fast the plume stretches in the vertical direction. This velocity in dimensionless form has been expressed through the fractional flow function. The physical velocity arises from this dimensionless velocity through a simple scaling relationship. This calculation leads to a rough, but straightforward, estimate of the plume propagation time. Accurate predictions of this time require knowledge of fluid and formation parameters. Simple calculations presented in this study suggest that the velocity of propagation of a plume of supercritical carbon dioxide may reach values of the order of tens of meters per year in an aquifer whose permeability is of the order of 100 millidarcy.

At the beginning, the main part of the plume has much higher gas saturation than the leading top part. This zone of highest gas saturation is bounded from above and below by two traveling-wave saturation profiles moving toward each other. Both traveling waves are followed by rarefaction waves. The top rarefaction wave includes a point where the saturation does not change in time. Surprisingly, this point corresponds to the most intense fluid flow. Although the total volumetric fluid flow is identically zero in the plume, the magnitudes of the individual Darcy velocities of gas and water reach their maximal value. This point also serves as a separator between the part of the plume above it, where the fluid displacement is drainage, and below, where the displacement mechanism is imbibition.

If there is a sequence of plumes one above the other, the lower plume propagates with a higher velocity and there is a possibility of plume coalescence.

Accurate prediction of plume migration requires good understanding of the formation properties, including capillary pressure and relative permeability functions. A new parametrization of the capillary pressure has been developed to achieve a good fit of laboratory core flood measurements for the Frio sandstone.

At depths and length scales, where gas compressibility cannot be neglected, the model described here needs a modification, which is beyond the scope of this work.

Acknowledgments This work was supported by the U.S. Department of Energy's Assistant Secretary for Coal through the Zero Emission Research and Technology Program under US Department of Energy contract no. DE-AC02-05CH11231 to Lawrence Berkeley National Laboratory. The authors thank Prof. Ruben Juanes of Massachusetts Institute of Technology for very inspiring discussions. The authors are grateful to Dr. Christine Doughty and Dr. Karsten Pruess of Lawrence Berkeley National Laboratory for a thorough review of the manuscript and valuable suggestions, which helped to improve the presentation.

Appendix A

Here, we present the formulae used for the relative permeability and capillary pressure functions in the calculations discussed above.

The parameters characterizing the fluid and rock properties are listed in Table 1. The fluid properties roughly correspond to the properties of water and supercritical CO_2 at the temperature of 60°C and pressure of 150 bars.

Accurate estimation of the transition zone in a traveling-wave solution requires high-quality fitting of the plateau zone on the capillary pressure curve. In this study, we have used the following parametrization for the Leverett's $\mathcal{J}$-function:

$$\mathcal{J}(S) = A\left(S_*^{-\lambda_1} - 1\right) + B\left(1 - S_*^{\lambda_2}\right)^{1/\lambda_2} \tag{A.1}$$

Here, A, B, and $\lambda_{1,2}$ are fitting parameters, and

$$S_* = \frac{S - S_\mathrm{J}}{1 - S_\mathrm{J}} \tag{A.2}$$

with another fitting parameter S_J. It turns out that this parametrization makes possible a significantly better fitting of experimental data for Frio and Berea sandstone than the traditionally used van Genuchten parametrization (Van Genuchten 1980).

The following set of parameters has been used in Fig. 8 to parameterize the experimental curve obtained from a drainage experiment on a Frio formation sandstone core involving supercritical CO_2 and brine:

$$\begin{aligned} A &= 0.0038 \\ B &= 0.28 \\ \lambda_1 &= 3.8 \\ \lambda_2 &= 5.18 \\ S_J &= 0.06 \end{aligned} \tag{A.3}$$

For the gas relative permeability, a Corey type formula (Corey 1954) has been used:

$$k_\mathrm{rg}(S) = (1 - \widetilde{S})^2(1 - \widetilde{S}^2) \tag{A.4}$$

where

$$\widetilde{S} = \frac{S - S_\mathrm{iw}}{1 - S_\mathrm{rg} - S_\mathrm{iw}} \tag{A.5}$$

In this work, the value of $S_\mathrm{rg} = 0.05$ has been used.

For water relative permeability, a van Genuchten function has been used

$$k_\mathrm{rw}(S) = \sqrt{S^*}\left[1 - \left(1 - S^{*1/\lambda}\right)^{\lambda}\right]^2 \tag{A.6}$$

where $S^* = S^*(S)$ is defined in

$$S^* = \frac{S - S_{\mathrm{iw}}}{1 - S_{\mathrm{iw}}} \tag{A.7}$$

The numerical values of the parameters for the relative permeability functions have been borrowed from Xu et al. (2005).

Appendix B: Traveling-Wave and Rarefaction-Wave Solutions

Traveling-Wave Solution

Let v be the velocity of traveling-wave propagation. Then, we seek a solution, which can be presented as a function of a single composite variable $Z = z - tv$. From Eq. 13,

$$v\phi S' = \frac{k}{\mu_{\mathrm{w}}}\left(f(S)\left(\frac{\mathrm{d}p_{\mathrm{c}}(S)}{\mathrm{d}S}S' - (\varrho_{\mathrm{w}} - \varrho_{\mathrm{g}})g\right)\right)' \tag{B.1}$$

Here, the prime denotes the derivative with respect to the composite variable Z. Define dimensionless plume propagation velocity V as

$$V = \frac{\mu_{\mathrm{w}}}{k(\varrho_{\mathrm{w}} - \varrho_{\mathrm{g}})g}v \tag{B.2}$$

Then, in dimensionless variables, we seek a solution in the form

$$S(\zeta, \tau) = S(\xi) \tag{B.3}$$

where

$$\xi = \zeta - \tau V \tag{B.4}$$

A dimensionless traveling-wave solution satisfies the equation

$$\phi V\frac{\mathrm{d}S}{\mathrm{d}\xi} - \frac{\mathrm{d}}{\mathrm{d}\xi}\left(f(S)\left(\gamma\mathcal{J}'(S)\frac{\mathrm{d}S}{\mathrm{d}\xi} - 1\right)\right) = 0 \tag{B.5}$$

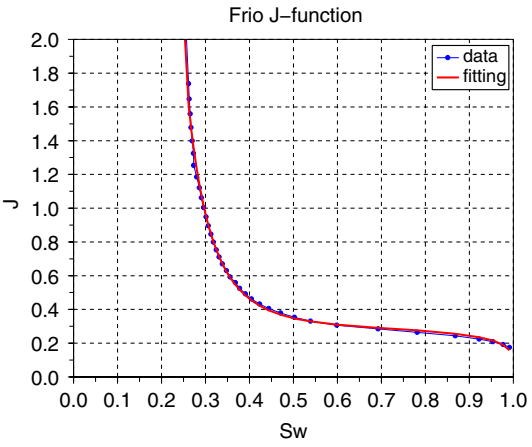

Fig. 8 The blue curve with circle markers is the data, and the red curve is the fitting curve. Fitting the plateau with the new parametrization

(cf. 20). The plume migration velocity, V, can be found from the following considerations. We assume that the saturations at a large distance are known:

$$S(-\infty) = S_1 \quad \text{and} \quad S(+\infty) = S_2 \tag{B.6}$$

The saturation profile stabilizes at a large distance, so that

$$\left.\frac{\mathrm{d}S}{\mathrm{d}\xi}\right|_{-\infty} = \left.\frac{\mathrm{d}S}{\mathrm{d}\xi}\right|_{+\infty} = 0 \tag{B.7}$$

Accounting for the boundary conditions (B.6 and B.7), integration of Eq. B.5 yields

$$V = -\frac{1}{\phi}\frac{f(S_2) - f(S_1)}{S_2 - S_1} \tag{B.8}$$

Physically, the latter equation is an expression of mass conservation.

If $S_2 < S_1$, then the traveling wave propagates upward (drainage), ($V > 0$), if $f(S_2) > f(S_1)$; it propagates downward (imbibition) if $f(S_2) < f(S_1)$. Conversely, if $S_2 > S_1$, the traveling wave propagates downward (imbibition) if $f(S_2) > f(S_1)$; it propagates upward (drainage) if $f(S_2) < f(S_1)$. An interesting case is a standing wave, which corresponds to the saturations S_1 and S_2, for which $f(S_2) = f(S_1)$ and $V = 0$.

By virtue of the Lagrange finite increments theorem, Eq. B.8 implies that

$$V = -\frac{1}{\phi}\, f'(S)\big|_{S=\widetilde{S}} \tag{B.9}$$

for some saturation $\widetilde{S}$ between S_1 and S_2. Therefore, the fastest traveling-wave propagation corresponds to a pair of saturations both close to the maximum of the absolute value of the derivative $f'(S)$. In a typical case, the function $f(S)$ has two intervals where it is convex, and one interval where it is concave (see Fig. 5). The maximum of the absolute value of $f'(S)$ is attained at a saturation where $f''(S) = 0$, i.e., at a dividing point between adjacent intervals of convexity and concavity.

Integration of Eq. B.5 from $-\infty$ to ξ and from ξ to $+\infty$ yields

$$\phi V(S(\xi) - S_1) = \gamma f(S)\mathcal{J}'(S)\frac{\mathrm{d}S}{\mathrm{d}\xi} - f(S(\xi)) + f(S_1) \tag{B.10}$$

$$\phi V(S_2 - S(\xi)) = -\gamma f(S)\mathcal{J}'(S)\frac{\mathrm{d}S}{\mathrm{d}\xi} + f(S(\xi)) - f(S_2) \tag{B.11}$$

Explicit solutions to the last two equations can be obtained in the form $\xi = \xi(S)$:

$$\frac{\mathrm{d}\xi}{\mathrm{d}S} = \frac{\gamma f(S)\mathcal{J}'(S)}{f(S) - f(S_1) - \dfrac{f(S_2) - f(S_1)}{S_2 - S_1}(S - S_1)} \tag{B.12}$$

$$\frac{\mathrm{d}\xi}{\mathrm{d}S} = \frac{\gamma f(S)\mathcal{J}'(S)}{f(S) - f(S_2) - \dfrac{f(S_2) - f(S_1)}{S_2 - S_1}(S - S_2)} \tag{B.13}$$

One can verify that Eqs. B.12 and B.13 are equivalent. Moreover, the denominator in either equation is the difference between $f(S)$ and a linear interpolation between $f(S_1)$ and $f(S_2)$. Therefore, the denominator vanishes both at $S = S_1$ and $S = S_2$. A traveling-wave solution can be obtained by explicit integration of either one of the Eqs. B.12 and B.13 if the denominator does not vanish between S_1 and S_2. For example, this holds true if both S_1 and S_2

are in the same interval of convexity or concavity of the function $f(S)$. A solution $\xi(S)$ is determined up to a vertical shift of the coordinate. Let us pick a saturation value S_0 between S_1 and S_2. Putting $\xi_0 = \xi\,(S_0)$, one obtains

$$\xi(S) = \xi_0 + \int_{S_0}^{S} \frac{\gamma f(\eta)\mathcal{J}'(\eta)}{f(\eta) - f(S_1) - \dfrac{f(S_2) - f(S_1)}{S_2 - S_1}(\eta - S_1)}\,\mathrm{d}\eta \tag{B.14}$$

or, equivalently,

$$\xi(S) = \xi_0 + \int_{S_0}^{S} \frac{\gamma f(\eta)\mathcal{J}'(\eta)}{f(\eta) - f(S_2) - \dfrac{f(S_2) - f(S_1)}{S_2 - S_1}(\eta - S_2)}\,\mathrm{d}\eta \tag{B.15}$$

The function $\xi(S)$ characterizes the transition of the saturation between the two extreme values S_1 and S_2 in the propagating wave. The size of this transition zone is, in particular, determined by the structure of Leverett's $\mathcal{J}$-function and the dimensionless factor γ. A smaller surface tension coefficient or higher permeability result in a sharper transition front (see Eq. 19).

Rarefaction Wave

A rarefaction wave is a self-similar solution obtained for the hyperbolic approximation (25). The term comes from gas dynamics (Landau and Lifshitz 1959). In order to find such a solution, put

$$\eta = \frac{\zeta - \zeta_0}{\tau} \tag{B.16}$$

where ζ_0 is the location of the center of the wave. Then, Eq. 25 takes on the form

$$-\phi\eta = f'(S) \tag{B.17}$$

The last relationship provides a solution in the form $\eta = \eta(s)$ (cf. Eqs. B.14 and B.15).

Equation B.17 can be converted into $S = S(\eta)$ if the derivative $f'(S)$ is monotone with respect to S. In other words, the second derivative $f''(S)$ must not change the sign. In particular, the range of saturations in a rarefaction wave must be contained in a single interval of convexity or concavity.

In terms of variables ζ and τ, a self-similar solution is provided by

$$\zeta = \zeta_0 - \tau\frac{1}{\phi}f'\left(S(\tau, \zeta)\right) \tag{B.18}$$

In particular, the velocity of propagation of the part of the rarefaction wave, where brine saturation is S is equal to

$$V_{\mathrm{r}}(S) = -\frac{1}{\phi}f'\left(S\right) \tag{B.19}$$

References

Al-Futaisi, A., Patzek, T.W.: Impact of wettability on two-phase flow characteristics of sedimentary rock: quasi-static model. Water Resour. Res. **39**(2), 1042–1055 (2003)

Al-Futaisi, A., Patzek, T.W.: Secondary imbibition in NAPL-invaded mixed-wet sediments. J. Contam. Hydrol. **74**(1–4), 61–81 (2004)
Barenblatt, G.I., Gilman, A.A.: A mathematical model of non-equilibrium countercurrent capillary imbibition. Eng. Phys. J. **52**(3), 46–461 (1987)
Barenblatt, G.I., Entov, V.M., Ryzhik, V.M.: Theory of Fluid Flows through Natural Rocks. Kluwer Academic Publishers, Dordrecht (1990)
Bedrikovetsky, P., De Deus, J., Eurico Altoé, J.: Secondary migration of oil: analytical model. SPE 69411. In: 2001 SPE Latin American and Carribean petroleum engineering conference, Buenos Aires, Argentina, SPE (2001)
Bryant, S.L., Lakshminarasimhan, S., Pope, G.A.: Buoyancy dominated multiphase flow and its impact on geological sequestration of CO_2, SPE 99938. In: 2006 SPE/DOE symposium on improved oil recovery,Tulsa, OK, SPE, 22–26 April 2006
Buckley, S.E., Leverett, M.C.: Mechanisms of fluid displacement in sands. Trans. AIME **146**, 149–158 (1942)
Corey, A.T.: The interrelations between gas and oil relative permeabilities. Producers Mon. **19**, 38–41 (1954)
Crandall, M.G., Evans, L.C., Lions, P.-L.: Some properties of viscosity solutions of Hamilton–Jacobi equations. Trans. Am. Math. Soc. **282**, 487–502 (1984)
Daley, T.M., Solbau, R.D., Ajo-Franklin, J.B., Benson, S.M.: Continuous active-source seismic monitoring of CO_2 injection in a brine aquifer. Geophysics **72**(5), A57–A61 (2007)
Doughty, C.: Modeling geologic storage of carbon dioxide: comparison of non-hysteretic and hysteretic characteristic curves. In: Energy conversion and management. Lawrence Berkeley National Laboratory, Berkeley, CA (2007)
Doughty, C., Myer, L.R.: Scoping calculations on leakage of CO_2 in geologic storage. In: McPherson, B., Sundquist, E. (eds.) Science and Technology of Carbon Sequestration. American Geophysical Union, Washington (2008)
Doughty, C., Freifeld, B.M., Trautz, R.C.: Site characterization for CO_2 geologic storage and vice versa: the Frio brine pilot, Texas, USA as a case study. Environ. Geol. (2008, in print)
Gasda, S.E., Bachu, S., Celia, M.A.: The potential for CO_2 leakage from storage sites in geological media: analysis of well distribution in mature sedimentary basins. Environ. Geol. **46**(6–7), 707–720 (2004)
Hubbert, M.K.: Entrapment of petroleum under hydrodynamic conditions. Bull. Am. Assoc. Petrol. Geol. **37**(8), 188–200 (1953)
Hubbert, M.K.: Darcy's law and the field equations of the flow of underground fluids. Trans. AIME **207**(7), 222–239 (1956)
Homsy, G.M.: Viscous fingering in porous media. Annu. Rev. Fluid Mech. **19**, 271–311 (1987)
IPCC.: Intergovernmental Panel on Climate Change Special Report on Carbon Dioxide Capture and Storage. Cambridge University Press, Cambridge (2005)
Landau, L.D., Lifshitz, E.M.: Course of Theoretical Physics. Fluid Mechanics. Series in Advanced Physics, vol. 6. Addison-Wesley, Reading (1959)
Leverett, M.C.: Capillary behavior in porous solids. Trans. AIME **142**, 152–169 (1941)
Leverett, M.C., Lewis, W.B., True, M.E.: Dimensional-model studies of oil-field behavior. Trans. AIME **146**, 175–193 (1942)
Lindeberg, E.: Escape of CO_2 from aquifers. Energy Convers. Manage. **38**, 235–240 (1997)
Luan, Z.-A.: Some theoretical aspects of gravity drainage in naturally fractured reservoirs, SPE 28641. In: 69th SPE annual technical conference and exhibition, pp. 357–366. New Orleans, LA, SPE (1994)
Mattax, C.C., Kyte, J.R.: Imbibition oil recovery from fractured, water-drive reservoir. SPE J. **2**, 177–184 (1962)
Muskat, M.: Physical Principles of Oil Production. McGraw-Hill, New York (1949)
Nordbotten, J.M., Celia, M.A., Bachu, S.: Injection and storage of CO_2 in deep saline aquifers: analytical solution for CO_2 plume evolution during injection. Transp. Porous Media **58**(3), 339–360 (2005)
Rapoport, L.A.: Scaling laws for use in design and operation of water-oil flow models. Trans. AIME **204**, 143–150 (1955)
Riaz, A., Tchelepi, H.A.: Dynamics of vertical displacement in porous media associated with CO_2 sequestration. SPE paper 103169. In: 2006 SPE annual technical conference and exhibition, San Antonio, TX, September 24–27, SPE (2006)
Rockafellar, R.T.: Convex Analysis. Princeton University Press, Princeton (1970)
Ryzhik, V.M.: On capillary imbibibtion by water of an oil-saturated reservoir. Soviet Acad. Izvestia Mech. Gas Fluids **2**, 149–151 (1960)
Saffman, P.G., Taylor, G.: The penetration of a fluid into a porous medium or Hele-Shaw cell containing a more viscous fluid. Proc. R. Soc. Lond. Ser. A. Math. Phys. Sci. **245**(1242), 312–329 (1958)
Shvidler, M.I., Levi, B.I.: One-dimensional filtration of immiscible fluids. Nedra, Moscow (1970) (in Russian)

Siddique F.I., Lake L.W.: A comprehensive dynamic theory of hydrocarbon migration and trapping SPE 38682. In: 1997 72th annual technical conference and exhibition, San Antonio, TX, SPE (1997)

Silin, D.B.: Generalizing Hopf and Lax-Oleĭnik formulae via conjugate integral. Monatsh. Mathe. **124**, 343–364 (1997)

Silin, D.B.: Viscosity solutions via unbounded set-valued integration. Nonlinear Anal. Theory Methods Appl. **31**(1–2), 55–90 (1998)

Silin, D.B., Patzek, T.W.: On Barenblatt's model of spontaneous countercurrent imbibition. Transp. Porous Media **54**(3), 297–322 (2004)

Van Genuchten, M.Th.: A closed-form equation for predicting the hydraulic conductivity of unsaturated soils. Soil Sci. Soc. Am. J. **44**(5), 892–898 (1980)

Xu, T., Apps, J.A., Pruess, K.: Mineral sequestration of carbon dixoide in a sandstone-shale system. Chem. Geol. **217**(3-4), 295–318 (2005)